Flow boiling heat transfer of zeotropic mixture refrigerants R454B and R449A in a smooth horizontal tube

Yu Xia[b], Jian Yu[a,b], Dilara Suulker[b], Hua Sheng Wang[b*]

[a]Super Radiator Coils, Ltd., 451 Southlake Blvd., Richmond, VA 23236, USA
[b]School of Engineering and Materials Science, Queen Mary University of London, Mile End Road, London E1 4NS, UK

Abstract

The paper reports an experimental investigation of local saturated flow boiling heat transfer of two environmentally-friendly zeotropic mixture refrigerants – R454B and R449A – in a horizontal 8.7 mm ID smooth tube, under high pressure and high heat-flux conditions. The test section is divided into five subsections to obtain quasi-local heat transfer and the refrigerants are heated by hot water in counter-current flow. For R454B, mass flux varied from 201 kg m^{-2} s^{-1} to 269 kg m^{-2} s^{-1} and the inlet pressure varied from 1.691 MPa to 3.282 MPa. For R449A, mass flux varied from 178 kg m^{-2} s^{-1} to 328 kg m^{-2} s^{-1} and the inlet pressure varied from 1.449 MPa to 3.244 MPa. The temperature glide and composition shift during flow boiling due to volatility difference between components were investigated. R454B and R449A displayed a temperature glide respectively from 1.12 K to 1.33 K and from 3.04 K to 4.61 K at the inlet of the test section. During the process of saturated boiling, for R454B, mass fraction of the less volatile component, R1234yf, in liquid phase was over 7% more than that in vapor phase. For R449A, mass fractions of the less volatile components, R134a and R1234yf, in liquid phase were around 6% and 4% more than those in vapor phase. Thermal resistance and mass transfer resistance were discussed. Before the occurrence of partial dry-out, heat-transfer coefficients of R454B were mainly located between 6.5 kW m^{-2} K^{-1} and 10 kW m^{-2} K^{-1} while most of data of R449A lay in the range of 3.5- 8 kW m^{-2} K^{-1}. The results of heat-transfer coefficient indicate that R454B exhibited greater heat transfer than R449A under close operating conditions. For both refrigerants, the heat transfer performance was locally enhanced in the region of near-zero vapor quality and gradually declines before intermediate vapor quality. After intermediate vapor quality, it tended to rise with vapor quality until a dramatic fall due to partial dry-out.

Keywords:

Zeotropic mixture refrigerant, GWP, Flow boiling, Green refrigerant, Refrigeration, Measurement, Heat pump

Nomenclature

A	area, m^2

c_{p}	isobaric specific heat capacity, J kg^{-1} K^{-1}
CF	coverage factor
COP	coefficient of performance
d_{i}	tube inner diameter, m
d_{o}	tube outer diameter, m
G	mass flux, kg m^{-2} s^{-1}
h	specific enthalpy, J kg^{-1}
h_{lv}	latent heat, J kg^{-1}
k_i	parameters in the law of propagation of error
$\dot{m}$	mass flow rate, kg s^{-1}
M	molecular mass, kg kmol^{-1}
P	pressure, Pa
Pr	Prandtl number
q	heat flux, W m^{-2}
Q	heat transfer rate, W
T	temperature, K
$\dot{V}$	volumetric flow rate, m^3 s^{-1}
X	circulation composition by mass/composition by mass in liquid phase
Y	composition by mass in vapor phase
Δz	length of subsection of the test section, m

Greek symbols

α	heat-transfer coefficient, W m^{-2} K^{-1}
δ	uncertainty
η	heat balance correction factor
λ	thermal conductivity, mW m^{-1} K^{-1}
μ	dynamic viscosity, μPa·s
ρ	density, kg m^{-3}
σ	surface tension, mN m^{-1}
χ	thermodynamic equilibrium vapor quality
Δh	specific enthalpy difference, J kg^{-1}
Δp	pressure drop, Pa
Δz	length of subsection of the test section, m

Subscripts

1, 2, 3, 4, 5	subsections 1, 2, 3, 4, 5
b	bubble point
c	circulation
d	dew point
eqm	equilibrium
H_2O	water
i	inner
in	inlet
l	liquid
mea	measured
v	vapor
out	outlet
r	refrigerant
sat	saturation
w	wall

1. Introduction

Since 2010s, constraints on global warming potential (GWP) led us to embrace the 'Fourth Generation refrigerants' and the demands for these refrigerants have been lifted to be: low-toxicity, non-flammability, stability, low GWP as well as other desired thermodynamic properties. However, single-constituent refrigerants hardly satisfy all these criteria, and some trade-offs between system performance and environmental protection are inevitable [1-4]. Thus, there has been an increasing number of studies on the development of new synthetic refrigerants as alternatives to conventional single-constituent refrigerants in various applications. It was reported that from 2014 to 2018, 35 new candidates received ASHRAE designations and safety classifications but only 5 of those were single-constitution refrigerants [5], illustrating how today's refrigerant development is dominated by newly-developed mixtures.

Since its invention by Honeywell and Chemours in 2008, R1234yf (2,3,3,3-etrafluoropropeneare) has attracted great interest as an ingredient for blending into conventional refrigerants to form new zeotropic mixtures. This interest is due to:

Its benefits:

1) Mixing R1234yf into another conventional refrigerants can lessen the GWP of mixtures.

2) The temperature glide of zeotropic mixtures can help optimize system performance by lowering thermodynamic irreversibility in organic Rankine cycle (ORC) and heat exchanger [6-9].
3) Some desirable thermodynamic properties can be achieved through flexible mixing between components.

Its challenges:

1) Inferior heat transfer capacity and *COP* associated with R1234yf and R1234yf-based mixtures [10-13] prompt more research on how to enhance system performance.
2) Introducing zeotropic mixture into systems will lead to a supplementary degree of freedom because of the temperature glide (non-isothermal phase change) and composition shift (non-constant concentration) phenomena. Compared to single-constituent refrigerants, more complex two-phase heat transfer and mass transfer will be encountered.
3) Studies on heat-transfer coefficient during non-isothermal two-phase region are inadequate.

To date, only a few earlier research efforts on some of R1234yf-based mixtures have been carried out.

Li et al. [13] attempted to explore heat transfer characteristics of binary mixtures of R1234yf and R32 at two mass fractions (50/50 and 80/20 by mass%) in a 2 mm inner diameter smooth horizontal tube. Their heat-transfer coefficient data collected under a variety of working conditions show that heat transfer performance varies significantly as the mass fraction of R32 increases in the mixture. Their results indicated a strong influence of temperature glide and mass transfer resistance due to inhomogeneity of consistency in zeotropic mixtures on heat transfer.

Jige et al. [4] experimentally investigated flow boiling heat transfer and pressure drop of R1234yf/R32 in horizontal multi-minichannels at two circulation compositions (50/50 and 80/20 by mass%). Heat transfer degradation compared to single-constituent refrigerants due to temperature glide and mass transfer resistance was observed and their results revealed that mass transfer resistance drops as vapor quality increases. They claimed that the less volatile component enriches in liquid due to preferential evaporation of the more volatile component, thus, the effective temperature difference available for heat transfer diminishes.

To better understand multi-component R1234yf-based blends, Mastrullo et al. [9] studied flow boiling heat transfer of a ternary zeotropic mixture, R452A, in a 6 mm ID horizontal tube. The experimental results of R452A were compared to those of conventional refrigerant R404A. Their data identified that these two refrigerants perform similarly in terms of heat transfer in a high-mass-flux condition while under a low-mass-flux condition, R404A exhibits higher heat-transfer coefficient. These differences may be explained by the fact that R452B and R404A share similar thermodynamic

and transport properties, but R452B's higher mass transfer resistance caused by its larger temperature glide limits the nuclear boiling contribution.

Lillo et al. [14] experimentally investigated the heat transfer and pressure drop of R448A, a quinary zeotropic mixture, and compared with R404A. R448A has a larger temperature glide than R404A at all working conditions, despite the fact that R448A has widely been regarded as a drop-in replacement to R404A. They observed that in the low-quality region R404A shows higher heat-transfer coefficients than R448A while in the high-quality region R448A shows higher heat-transfer coefficients than R404A.

Berto et al. [15] studied flow boiling heat transfer of two R1234yf-based ternary zeotropic blends in 8.0-mm and 0.96-mm ID smooth tubes. The refrigerants used are R455A (R32/R1234yf/R744 at 21.5/75.5/3 by mass%) and R452B (R32/R1234yf/R125 at 67/26/7 by mass%). Their data of R452B show considerably superior heat transfer than R455A, which is presumably due to thermodynamic properties and lower temperature glide and consequently lower mass transfer resistance.

R454B (Opteon XL41) and R449A (Opteon XP40) are two commercial R1234yf-based mixtures with lower GWP, both of which recently received ASHRAE designations. R454B is a binary mixture containing 68.9% of R32 and 31.1% of R1234yf by mass. It was developed to replace R410A. It is characterized by 78 % less GWP_{100} than R410A. R449A (1400 GWP_{100}) is a higher-order mixture (quaternary) including R-32, R125, R1234yf and R134a (24.3%, 24.7%, 25.3% and 25.7 % by mass), as a drop-in alternative to R404A and R507. It is seen that two-phase flow heat transfer and mass transfer characteristics at high pressure and high heat flux are far from well understood, which adversely limits their wide application in ORC, heat pumps and refrigeration systems. Relevant studies on local heat-transfer coefficient and pressure drop to inform future industrial applications are still in urgent need.

This paper presents an experimental study to shed light on flow boiling heat transfer of R454B and R449A under high pressure and high heat flux conditions inside a horizontal smooth tube with 8.7-mm inner diameter. It is anticipated to advance the understanding of temperature glide and composition shift phenomena involved in flow boiling process of these blends.

2. Experiment

The apparatus and test section are described below. The data reduction method and uncertainty analysis are presented.

2.1 Apparatus

Fig.1 shows the schematic of the apparatus. The system is composed of three loops: the refrigerant loop and two auxiliary loops (chilled water and heating water). In the refrigerant loop (green line), a

refrigerant mixture is circulated by an oil-free variable-speed magnetic pump and a micro motion mass flow meter is employed to measure the flow rate. In all runs, the refrigerant was pumped into the test section as subcooled liquid and an electrical pre-heater as well as two water pre-heater units are used to adjust the degree of subcooling. The combination of the electrical pre-heater and two water pre-heater units provides uniform heating, which can help avoid potential subcooled boiling and oscillation. In the test section, the refrigerant is evaporated by receiving heat from counter-current hot water. After the test section, the refrigerant is fully condensed to a sub-cooled liquid state by condensers and post-condensers before going back to the pump. In order to protect the pump, a bypass can recirculate a portion of the subcooled refrigerant to adjust the subcooling degree and the flow rate of refrigerant entering the pump. After the sub-cooler, a refrigerant receiver is connected in parallel, which is used to control the system pressure by altering the amount of refrigerant in the loop. The desired test pressure in the loop is achieved by the balance between the receiver, condensers and bypass valve. As shown in Fig.1, several sets of pressure transducers and T-type thermocouples are placed along the loop to monitor the variations of pressures and temperatures. In terms of the heating water loop, heating water from a thermal bath is delivered to the test section as a heat source designed to promote boiling of the refrigerant. The control of the water temperature is assigned to the thermal bath. Chilled water from a chiller mixed with ethylene glycol is supplied to the post-condenser units and sub-cooler units. The water flow rates in two auxiliary loops are measured by turbine flow meters. A condensation bypass is reserved for condensation experiments.

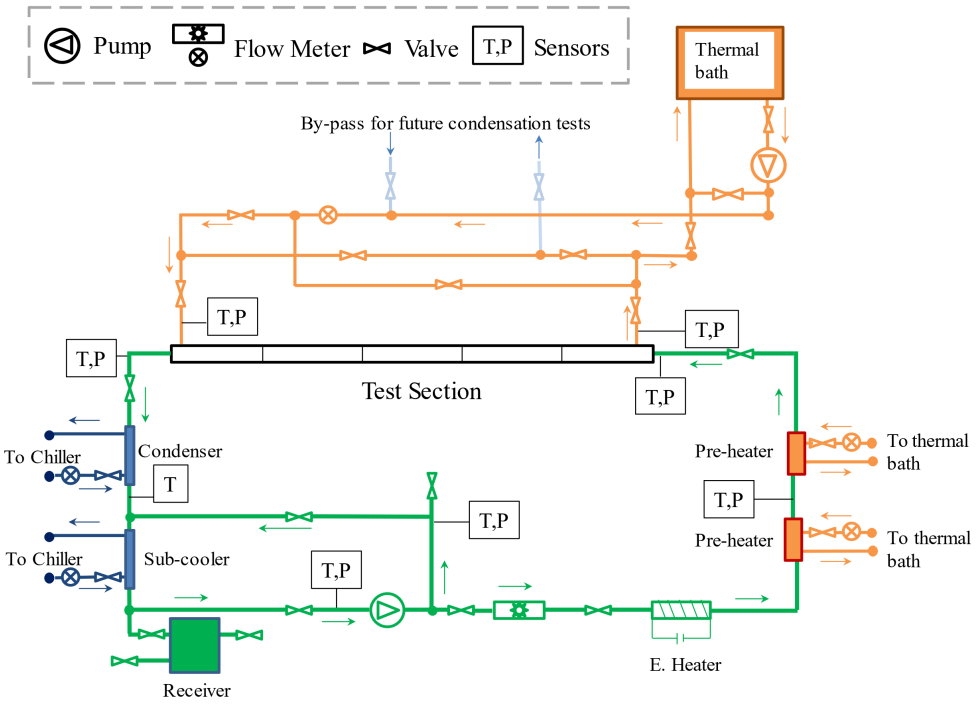

Fig.1 Schematic of the apparatus

Fig.2 illustrates the test section, which is made of a copper refrigerant-to-water counter-current flow tube-in-tube heat exchanger. Refrigerant flows inside the smooth tube with inner diameter equal to 8.7 mm and outer diameter equal to 9.5 mm. In order to obtain quasi-local heat transfer, the test section is divided into five subsections. Pressure and bulk-mean-temperature of refrigerants are measured at the inlet and outlet of the test section to determine the enthalpies. The pressure drop across each subsection is measured by differential pressure transducers. The wall temperature is obtained by eight T-type thermocouples embedded separately in the top, bottom, right, and left of the tube wall around the centre of each subsection. In addition, at the outlet of each subsection, the refrigerant temperatures are measured by resistance temperature detectors (RTDs) along the test section for reference. These measured refrigerant temperatures are compared with the calculated refrigerant temperatures which are functions of measured local pressure, local enthalpy and circulation composition of mixtures. Fig.2 also illustrates the passage for water in the test section. Heating water provided by the thermal bath flows within the annulus, counter to the direction of the refrigerant flow. Temperatures and pressures of heating water are measured at the entrance and exit of external annular water passage in the test section to calculate heat balance between the water and refrigerant sides. RTDs are installed along the external annulus to obtain the temperature drop of heating water across each subsection. As shown in Fig.3, the entire test section is properly insulated. Table 1 lists the main components and their characteristics.

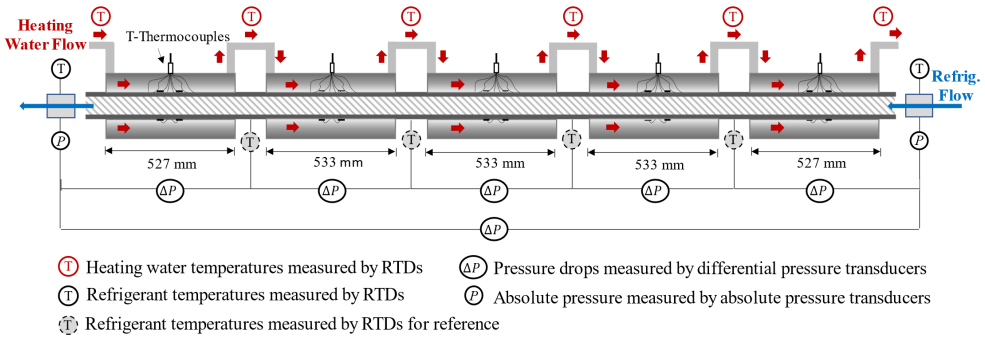

Fig.2 Detailed schematic of the test section

Fig.3 Apparatus after insulation

Table 1 List of main components and their characteristics

Main components	Description
Refrigerant loop	
Oil-free variable-speed magnetic pump	Circulating refrigerant in the refrigerant loop
Heat exchangers	As pre-heaters and condensers
E-heater	Adjusting thermodynamic state of refrigerants
Micro motion mass flow meter	Measuring flow rates of refrigerants
Refrigerant receiver	Storage of refrigerants; adjusting system pressure
Water loop	
Thermal bath	Controlling heating water temperature
Chiller	Providing chilled water for condensers
pumps	Circulating water in the water loop
Turbine flow meters	Measuring water flow rates
Absolute pressure transducers	Measuring absolute pressures
Temperature and pressure measurements	
Pt1000 RTDs	Measuring temperatures
T-type thermocouples	Measuring temperatures
Absolute pressure transducers	Obtaining absolute pressures
Differential pressure transducers	Obtaining pressure drop
Data-logger	Acquisition of experimental data

2.2 Data Reduction

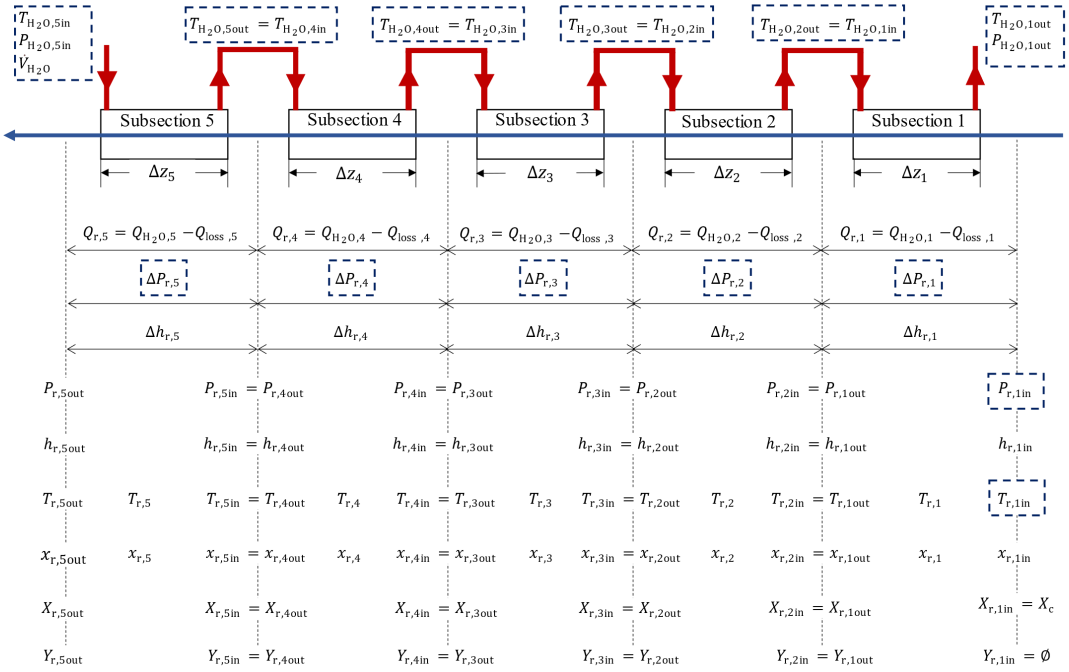

Fig.4 The data reduction methodology for this study (values in rectangle are measurements)

The data reduction process is demonstrated in Fig.4. A primary concern is to establish a pressure profile along the test tube. The pressure at the inlet of the test section (i.e. inlet of subsection 1) was measured with an absolute pressure transducer. It is widely accepted that pressure drop in the two-phase region is susceptible to change in vapor quality along the tube [7]. Thus, differential pressure transducers were used to measure pressure drops across each subsection instead of assuming a linear distribution across the entire test tube. Consequently, starting from the inlet of subsection 1, local absolute pressure at the inlet and outlet of each subsection can be worked out. The pressure profile is established as:

$$
\begin{aligned}
&P_{\mathrm{r,1in}} = \text{measurement} \\
&P_{\mathrm{r,2in}} = P_{\mathrm{r,1out}} = P_{\mathrm{r,1in}} - \Delta P_{\mathrm{r,1}} \\
&\vdots \\
&P_{\mathrm{r,5in}} = P_{\mathrm{r,4out}} = P_{\mathrm{r,4in}} - \Delta P_{\mathrm{r,4}} \\
&P_{\mathrm{r,5out}} = P_{\mathrm{r,5in}} - \Delta P_{\mathrm{r,5}}
\end{aligned} \tag{1}
$$

The refrigerant specific enthalpy at the inlet of subsection 1, $h_{\mathrm{r,1in}}$, is determined directly by the measured pressure, inlet temperature and circulation composition of the mixture at the inlet.

$$
h_{\mathrm{r,1in}} = f(P_{\mathrm{r,1in}}, T_{\mathrm{r,1in}}, X_{\mathrm{c}}) \tag{2}
$$

where X_c is the circulation composition of mixtures, i.e., composition of R449A and R454B in this case.

In the present work, the heat transfer rate to the refrigerant for each subsection is given by:

$$
\begin{aligned}
&Q_{r,1} = Q_{H_2O,1} - Q_{loss,1} \\
&Q_{H_2O,1} = \rho_{H_2O}\dot{V}_{H_2O}c_{pH_2O}\left(T_{H_2O,1in} - T_{H_2O,1out}\right) \\
&\vdots \\
&Q_{r,5} = Q_{H_2O,5} - Q_{loss,5} \\
&Q_{H_2O,5} = \rho_{H_2O}\dot{V}_{H_2O}c_{pH_2O}\left(T_{H_2O,5in} - T_{H_2O,5out}\right)
\end{aligned} \tag{3}
$$

where, ρ_{H_2O}, c_{pH_2O} and $\dot{V}_{H_2O}$ are the density, isobaric specific heat capacity and volumetric flow rate of heating water, respectively. Q_{loss} is the heat loss estimated by the temperature difference between heating water and ambient air temperatures, based on heat loss tests.

Starting from the inlet of subsection 1, subsequent refrigerant enthalpies at the outlet and inlet of each subsection are calculated using heat transfer rate for each subsection.

$$
\begin{aligned}
&h_{r,1out} = h_{r,2in} = h_{r,1in} + (Q_{r,1}/\dot{m}_r) \\
&\vdots \\
&h_{r,4out} = h_{r,5in} = h_{r,4in} + (Q_{r,4}/\dot{m}_r) \\
&h_{r,5out} = h_{r,5in} + (Q_{r,5}/\dot{m}_r)
\end{aligned} \tag{4}
$$

where, $\dot{m}_r$ is the refrigerant mass flow rate

The determination of refrigerant temperature significantly affects the calculation of the experimental heat-transfer coefficients of zeotropic refrigerant mixtures. In the present work, the refrigerant temperatures at the inlet and outlet of each subsection are determined from the local pressure, enthalpy and mixture composition by iteration using REFPROP 10.0 [16], assuming a thermodynamic equilibrium state. The representative refrigerant temperature of each subsection is defined as the arithmetic average of refrigerant temperatures at the inlet and outlet of each subsection by Eq. (5).

$$
\begin{aligned}
&T_{r,1} = \left[T_{r,1in} + T_{r,\,1out}\left(P_{r,1out}, h_{r,1out},\, X_c\right)_{eqm}\right]/2 \\
&T_{r,2} = \left[T_{r,2in}(P_{r,2in}, h_{r,2in},\, X_c)_{eqm} + T_{r,2out}\left(P_{r,2out}, h_{r,2out},\, X_c\right)_{eqm}\right]/2 \\
&\vdots \\
&T_{r,5} = \left[T_{r,5in}(P_{r,5in}, h_{r,5in},\, X_c)_{eqm} + T_{r,5out}(P_{r,5out}, h_{r,5out},\, X_c)_{eqm}\right]/2
\end{aligned} \tag{5}
$$

Note that $T_{r,1in}$ is measured temperature.

In addition, during experiments some RTDs were placed inside the test tube to directly measure refrigerant temperatures along the tube. Due to uncertainty in measurement and potential influence of temperature inhomogeneity at two sides of vapor-liquid interface [17,18], the measured refrigerant temperatures are only regarded as reference.

Similar to the representative temperature, the representative vapor quality of each subsection is determined by Eq.(6)

$$\chi_{\mathrm{r},1} = \left[\chi_{\mathrm{r},1\mathrm{in}}\left(P_{\mathrm{r},1\mathrm{in}}, T_{\mathrm{r},1\mathrm{in}}, X_{\mathrm{c}}\right)_{\mathrm{eqm}} + \chi_{\mathrm{r},1\mathrm{out}}\left(P_{\mathrm{r},1\mathrm{out}}, h_{\mathrm{r},1\mathrm{out}}, X_{\mathrm{c}}\right)_{\mathrm{eqm}}\right]/2$$

$$\chi_{\mathrm{r},2} = \left[\chi_{\mathrm{r},2\mathrm{in}}\left(P_{\mathrm{r},2\mathrm{in}}, h_{\mathrm{r},2\mathrm{in}}, X_{\mathrm{c}}\right)_{\mathrm{eqm}} + \chi_{\mathrm{r},2\mathrm{out}}\left(P_{\mathrm{r},2\mathrm{out}}, h_{\mathrm{r},2\mathrm{out}}, X_{\mathrm{c}}\right)_{\mathrm{eqm}}\right]/2$$

$$\vdots$$

$$\chi_{\mathrm{r},5} = \left[\chi_{\mathrm{r},5\mathrm{in}}\left(P_{\mathrm{r},5\mathrm{in}}, h_{\mathrm{r},5\mathrm{in}}, X_{\mathrm{c}}\right)_{\mathrm{eqm}} + \chi_{\mathrm{r},5\mathrm{out}}\left(P_{\mathrm{r},5\mathrm{out}}, h_{\mathrm{r},5\mathrm{out}}, X_{\mathrm{c}}\right)_{\mathrm{eqm}}\right]/2 \quad (6)$$

In addition, the local compositions of mixtures in the liquid phase X_{r} and the vapor phase Y_{r} at the inlet and outlet of each subsection are evaluated as:

$$X_{\mathrm{r},1\mathrm{in}} = X_{\mathrm{c}} \quad \text{(due to subcooled state)}$$

$$Y_{\mathrm{r},1\mathrm{in}} = \emptyset \quad \text{(due to subcooled state)}$$

$$X_{\mathrm{r},2\mathrm{in}} = X_{\mathrm{r},1\mathrm{out}} = f(P_{\mathrm{r},2\mathrm{in}}, h_{\mathrm{r},2\mathrm{in}}, X_{\mathrm{c}})_{\mathrm{eqm}}$$

$$Y_{\mathrm{r},2\mathrm{in}} = Y_{\mathrm{r},1\mathrm{out}} = f(P_{\mathrm{r},2\mathrm{in}}, h_{\mathrm{r},2\mathrm{in}}, X_{\mathrm{c}})_{\mathrm{eqm}}$$

$$\vdots$$

$$X_{\mathrm{r},5\mathrm{out}} = f(P_{\mathrm{r},5\mathrm{out}}, h_{\mathrm{r},5\mathrm{out}}, X_{\mathrm{c}})_{\mathrm{eqm}}$$

$$Y_{\mathrm{r},5\mathrm{out}} = f(P_{\mathrm{r},5\mathrm{out}}, h_{\mathrm{r},5\mathrm{out}}, X_{\mathrm{c}})_{\mathrm{eqm}} \quad (7)$$

The averaged heat flux and heat-transfer coefficient of a subsection are calculated by Eqs.(8) and (9).

$$q = \frac{Q_{\mathrm{r}}}{A} \quad (8)$$

$$\alpha = \frac{q}{T_{\mathrm{wi}} - T_{\mathrm{r}}} \quad (9)$$

where A is the heat transfer area of a subsection, T_{wi} denotes the representative inner tube surface temperature of a subsection and is obtained by the tube wall temperature, T_{wo}, with a correction of heat conduction.

$$T_{\mathrm{wi}} = T_{\mathrm{wo}} - \frac{Q_{\mathrm{r}}}{2\pi\lambda_{\mathrm{w}}\Delta z} ln \frac{d_{\mathrm{o}}}{d_{\mathrm{i}}} \quad (10)$$

where T_{wo} is determined by the measured temperatures at the top, bottom, right, and left, by eight

RTDs embedded in the tube wall.

$$T_{\mathrm{wo}} = \frac{T_{\mathrm{wo,top1}} + T_{\mathrm{wo,top2}} + T_{\mathrm{wo,bot1}} + T_{\mathrm{wo,bot2}} + T_{\mathrm{wo,right1}} + T_{\mathrm{wo,right2}} + T_{\mathrm{wo,left1}} + T_{\mathrm{wo,left2}}}{8} \tag{11}$$

Table 2 summarizes the thermodynamic and transport properties of R449A, R454B and four single-constituent refrigerants at 2.199 MPa are obtained using REFPROP 10.0 [16]. GWP_{100} values are obtained from 2018 Assessment Report by Refrigeration, Air Conditioning and Heat Pumps Technical Options Committee [5].

Table 2 Properties of saturated refrigerants from NIST REFPROP 10.0 [16] at 2.199 MPa

Refrigerant	R1234yf	R32	R125	R134a	R454B	R449A
T_{b},℃	-	-	-	-	38.22	47.27
T_{d},℃	-	-	-	-	39.52	51.29
T_{sat}, ℃	73.44	35.17	43.82	71.71	-	-
Glide, K	-	-	-	-	1.30	4.02
M, kg kmol^{-1}	114.04	52.024	120.02	102.03	62.614	87.213
ρ_{l}, kg m^{-3}	860.10	916.27	1057.8	985.60	923.46	984.99
ρ_{v}, kg m^{-3}	146.52	63.65	160.72	121.35	77.31	106.54
μ_{l} , μPa s	77.77	100.8	101.7	103.7	97.34	102.5
μ_{v} , μPa s	15.15	13.47	15.58	14.66	13.84	14.38
λ_{l}, mW m^{-1} K^{-1}	49.40	118.2	51.77	60.91	97.27	69.99
λ_{v}, mW m^{-1} K^{-1}	22.38	17.28	19.49	20.93	18.29	19.62
Pr_{l}	3.043	1.769	3.324	3.126	1.972	2.627
Pr_{v}	1.271	1.439	1.202	1.160	1.313	1.165
h_{lv}, kJ kg^{-1}	90.75	248.79	86.39	121.57	199.03	141.61
GWP_{100}	<1	704	3450	1360	490	1400

2.3 Uncertainty Analysis

It is worth noting that all properties have been calculated assuming nominal compositions of the refrigerants as circulation compositions in the present work. Table 3 lists the experimental uncertainty of the measured parameters. All instruments and sensors were properly calibrated. For each test run, when the system reached a steady-state condition, 60 readings of measurements (temperature, pressure and flow rate) were gathered in a 10-minute period and averaged. The combined uncertainties are calculated in accordance with the law of propagation of error analysis [19-21].

$$\delta(f) = \sqrt{\sum_{i=1}^{N} \left(\frac{\partial f}{\partial k_i}\delta(k_i)\right)^2} \tag{13}$$

A coverage factor $CF = 2$ is used to obtain an expanded uncertainty with a 95% confidence level. The uncertainty analysis in the present work was carried out referring to methodology presented in

Kondou et al. [18]. A description of uncertainty analysis with calculation procedure is given in Appendix. The expanded uncertainties are depicted as error bars in the figures along with the relevant experimental results. The uncertainty analysis has revealed that major contributions to the overall uncertainty of heat-transfer coefficient are uncertainty of heat flux and uncertainty associated with wall-to-refrigerant temperature difference.

Table 3 Uncertainties of measured parameters based on full scale.

Measurement	Instruments	Range	Accuracy
	Water side		
Water temperature (test section)	Pt1000 RTDs	1.7 to 82.2 ℃	±0.006℃
Water volumetric flow rate	Turbine Flow Meter	0.063 to 3.785 l s^{-1}	±0.5%
	Refrigerant side		
Refrig. temperatures (test section)	Pt1000 RTDs	-1.1 to 98.9℃	±0.006℃
Refrig.inlet absolute pressure (test section)	Absolute Pressure Transducer	0 to 51.71 bar	±0.25%
Refrig. pressure drop (across each subsection)	Differential Pressure Transducers	0 to 1.03 bar	±0.25%
Outer wall temperature	T-thermocouples	1.7 to 82.2℃	±0.01℃
Refrig. mass flow rate	Micro Motion Mass Flow Meter	0.01 kg s^{-1} to 0.1 kg s^{-1})	±0.2%

3. Results and discussion

Table 4 summaries the experimental conditions of R454B and R449A, respectively. All data were obtained at steady-state conditions.

Table 4 Summary of experimental conditions.

		G (kg $m^{-2}s^{-1}$)	P_{inlet} (MPa)	$T_{\mathrm{b,inlet}}$ (□)	$T_{\mathrm{d,inlet}}$ (□)	Subcooling (K)	$\chi\,(-)$ (two-phase region)
R454B	Test 1	200.99	2.424	42.27	43.53	9.42	0.266-0.952
	Test 2	246.94	1.691	27.81	29.14	6.39	0.354-0.897
	Test 3	259.27	3.156	53.73	54.87	12.96	0.278-0.810
	Test 4	260.19	3.189	54.18	55.32	13.35	0.275-0.808
	Test 5	261.66	3.282	55.48	56.60	15.13	0.189-0.877
	Test 6	269.04	2.235	38.90	40.19	7.17	0.426-0.973
R449A	Test 1	178.40	3.244	65.05	68.09	15.92	0.240-0.991
	Test 2	193.63	2.199	47.27	51.29	6.21	0.325-0.969
	Test 3	206.16	1.458	30.34	34.95	8.20	0.339-0.840
	Test 4	228.51	1.552	32.79	37.32	11.50	0.310-0.810

Test 5	272.32	1.449	30.08	34.69	10.33	0.365-0.910
Test 6	315.39	2.670	55.91	59.52	16.25	0.223-0.948
Test 7	327.99	2.239	48.04	52.03	14.64	0.281-0.983

3.1 Composition shift and temperature glide

It is widely accepted that, unlike single-constituent refrigerants, the phase changing process with zeotropic mixtures is non-isothermal at a given pressure due to different saturation temperatures of different constituents in mixtures. The local thermodynamic equilibrium temperature is a function of not only the local pressure but also local equilibrium compositions in liquid and vapor phases. In what follows, the variations of refrigerant temperature and local composition shift with the vapor quality for R454B and R449A are discussed respectively.

Composition shift

Fig. 5(a) shows the phase equilibrium of R32/R1234yf (Test 1 of R454B taken as an instance) in a three-dimensional way to illustrate a shift in composition for R454B along the process of flow boiling within the tube. In the light of pressure drop, the bubble and dew lines vary slightly streamwise. At the inlet, $X_{R32} = 0.689$ (i.e. $X_{R1234yf} = 0.311$) is the circulation composition of R454B. As boiling continues, the remaining refrigerant in liquid phase moves to states 1, 2, 3, 4 and till to be completely evaporated. In equilibrium, the generated vapor phase shifts to state 1', 2', 3', 4' correspondingly and returns to circulation composition of R454B by reaching a superheated state. For the sake of analysis, if we project this flow boiling process on a 2D surface by neglecting the variation of dew and bubble lines caused by pressure drop, Fig.5(b) can be obtained. It is apparent that, through the boiling process, the liquid phase contains more the less volatile constituent, R1234yf, than circulation composition of R454B, while the vapor phase is richer in the more volatile one, R32, than circulation composition. Specifically, during process of saturated boiling, mass fraction of R32 in the liquid phase is approximate 7% less than that in the vapor phase while mass fraction of R1234yf in the liquid phase is around 7% more than that in the vapor phase.

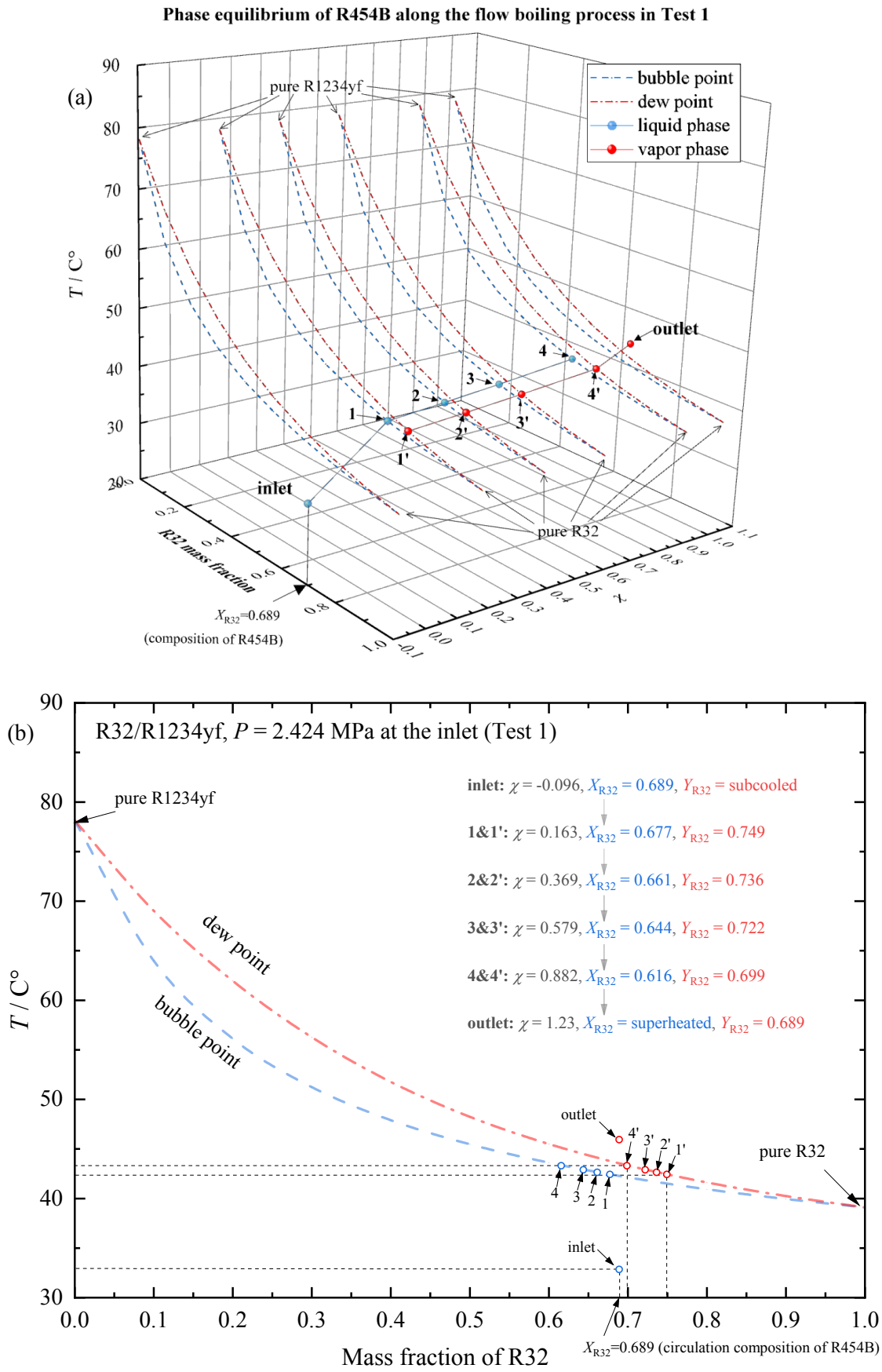

Fig.5 Composition shift of R454B in Test 1: (a) considering pressure drop (b) neglecting pressure drop.

In terms of R449A involving more than two constituents, it is not likely to demonstrate the composition shift of refrigerant in a similar way to R454B. Thus, Fig.6(a) is employed here to reflect composition shift of R449A (Test 2, as an example) in the liquid and vapor phases, respectively. During boiling, at a certain quality, the more volatile constituents, R32 and R125, are richer in the vapor phase than circulation composition while the less volatile constituents, R1234yf and R134a, tend to remain in the liquid phase. Fig.6(b) illustrates the mass fraction difference of vapor to liquid along flow boiling process. It can be seen that concentrations of R134a and R1234yf in the liquid phase are over 6% and 4% respectively more than those in the vapor phase while concentrations of R32 and R125 in the liquid phase are around 7% and 3% less than those in the vapor phase. The composition shift illustrated here suggests that a strong fraction gradient and associated mass transfer resistance may occur over the liquid-vapor interface due to volatility difference, which has been noted in earlier studies [7,18,22].

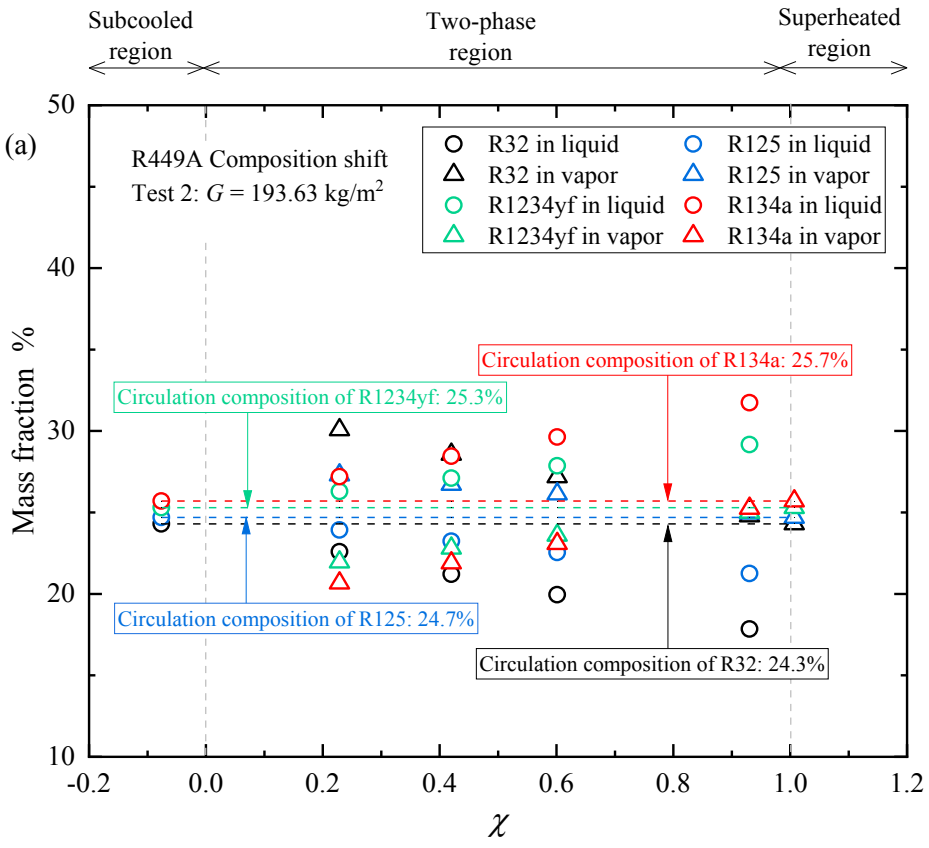

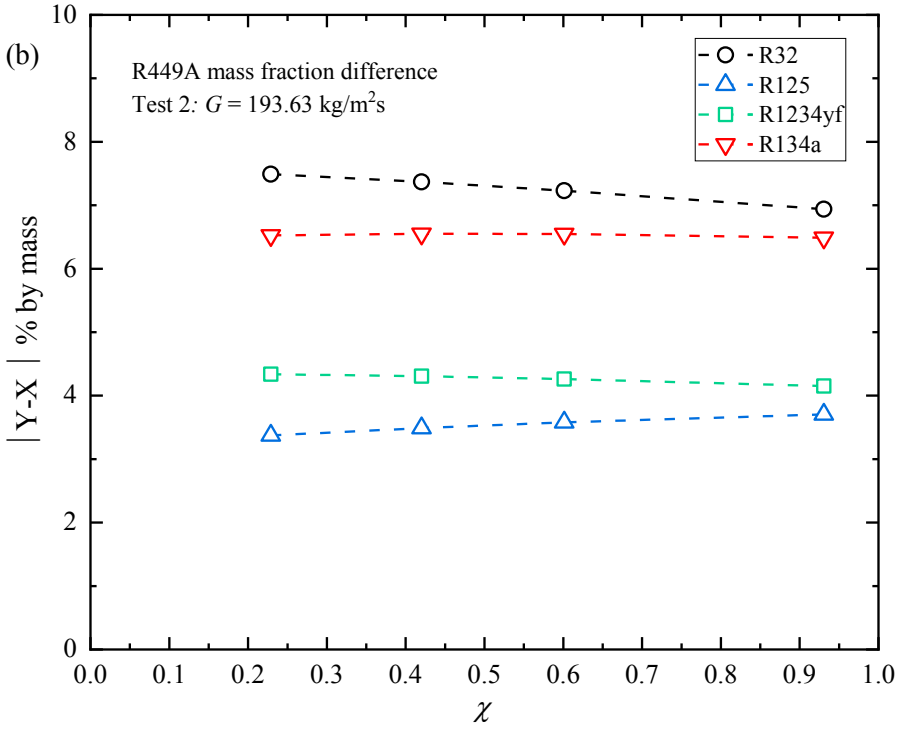

Fig.6 Composition shift of R449A under conditions of Test 2: (a) composition in liquid and vapor phase along flow boiling (b) mass fraction difference of liquid to vapor along flow boiling.

Temperature glide

Fig.7 reports dew and bubble temperatures profiles, calculated and measured refrigerant temperatures profile and pressure profile versus vapor quality for one test run performed with R454B and R449A. $T_{r,cal}$ refers to the calculated refrigerant temperature, $T_{r,mea}$ indicates the refrigerant temperature measured by RTDs regarded as reference. T_b and T_d are bubble temperature and dew temperature, which decline slightly due to pressure loss along the flow boiling process. P_z is the local pressure measured. An overall inspection of Fig.7(a) and Fig.7(b) confirms higher temperature glide of R449A than that of R454B. Under present experimental conditions, R454B displays a temperature glide in the range of 1.12 K to 1.33 K at the inlet, and the temperature glide for R449A varies from 3.04 K to 4.61 K at the inlet.

It can be observed that refrigerants enter the test section at a subcooled state and the temperature rises rapidly up to bubble point, then saturated boiling begins. During saturated boiling, as the boiling proceeds along the flow direction, the refrigerant temperature increases with vapor quality, which does not exist in saturated region of single-constituent refrigerants. To fully evaporate the refrigerant, additional sensible heat is required to heat the remaining liquid (rich in less volatile components) and vaporized gas (rich in more volatile components) to the higher dew point [7,18]. Correspondingly, a

considerable thermal resistance is also generated and coupled with the mass transfer resistance. Wherein, the fraction gradient suppresses the diffusion of the less volatile component in bulk liquid to the liquid-vapor interface while the temperature gradient inhibits temperature driving force from heated surface to interface.

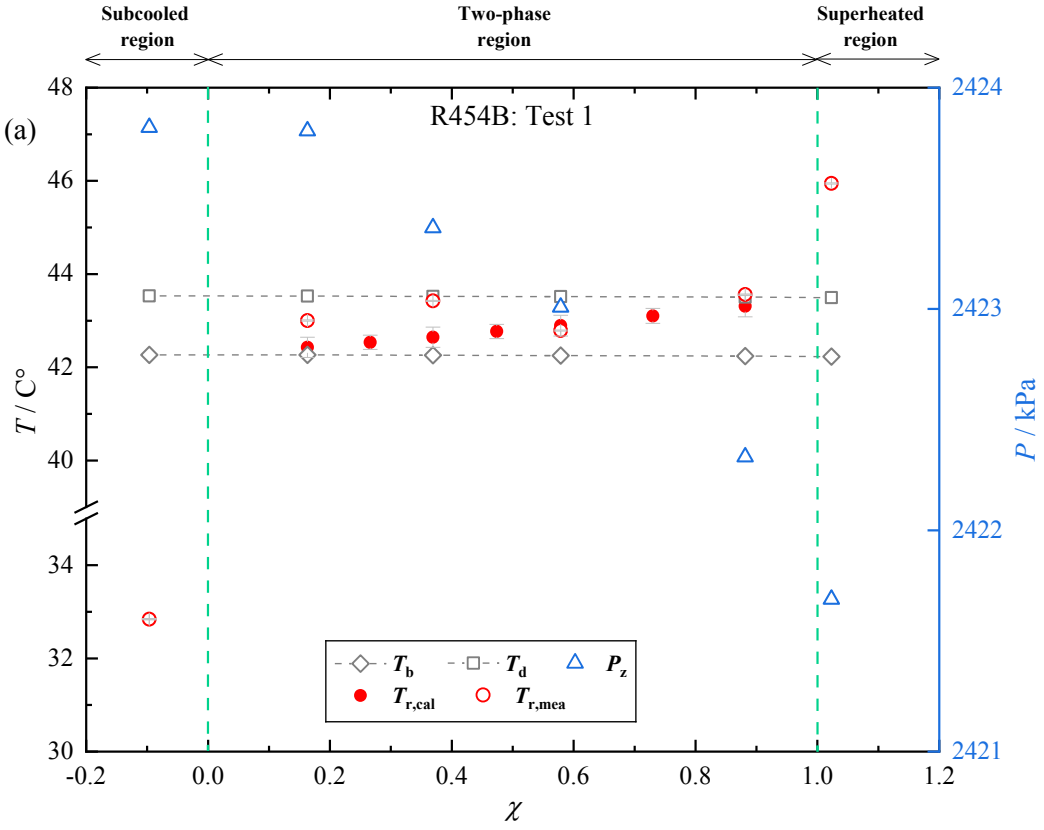

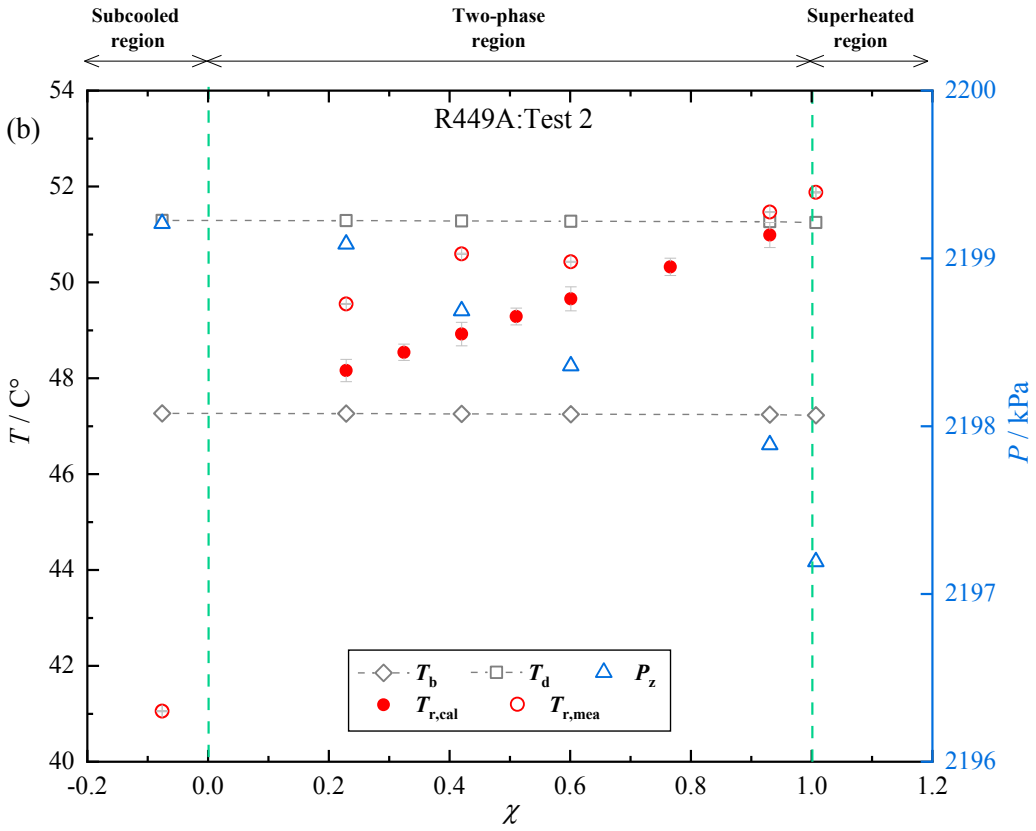

Fig.7 Refrigerant temperatures and local pressures vs vapor quality for R454B (Test1) and R449A (Test 2).

3.2 Heat transfer analysis

Heat-transfer coefficients of R454B and R449A versus vapor quality in saturated boiling region are plotted separately in Fig.8. The vertical bars indicate the expanded uncertainty at 95% confidence level and horizontal bars indicate the vapor quality change in each subsection. As shown in Fig.8, heat-transfer coefficients of R454B mainly range from 6.5 kWm^{-2} K^{-1} to 10 kW m^{-2} K^{-1} while most of data of R449A lie in the range of 3.5 to 8 kWm^{-2} K^{-1}, before a rapid decrease in high vapor quality region due to partial dry-out. Heat flux is plotted against vapor quality for these two mixtures in Fig.9. The vertical bars indicate the expanded uncertainty at 95% confidence level and the horizontal bars indicate the vapor quality change within each subsection. Closer inspection of Fig. 9 shows that heat flux of R454B approximately varies from 30 kW m^{-2} to 80 kW m^{-2} while heat flux of R449A approximately varies from 15 kW m^{-2} to 65 kW m^{-2}, if neglecting the dramatic decline owing to dry-out at high quality.

It is apparent that R454B exhibited a noticeably higher heat-transfer coefficient than R449A under similar experimental conditions, which is presumably ascribed to R454B's higher latent heat, higher liquid thermal conductivity, lower temperature glide, and smaller molecular mass. For both R454B and R449A, as a common trend, heat-transfer coefficient first declines gradually with a rise in vapor

quality, presenting a temporary minimum at low vapor quality. But when vapor quality becomes larger than 0.5, heat-transfer coefficient tends to increase with quality. After local peaking in the high-quality region, heat-transfer coefficient drops sharply due to onset of partial dry-out [23]. The trend is consistent with findings of Greco [24,25] under high heat flux and high-pressure working conditions. A further discussion of the trend can be divided into three parts streamwise.

Heat transfer peak in the near-zero quality region

An obvious peculiar behaviour is the occurrence of local heat-transfer enhancement in the region of near-zero equilibrium quality. As shown in Table 4, the refrigerant enters the test section at a subcooled condition in all tests. The refrigerant temperature then rises to its bubble point temperature. Subcooled boiling governs in the initial region until saturated boiling begins. A peak of heat-transfer coefficient occurs at transition to saturated boiling. This peculiar behaviour was also observed in some earlier experiments with some single-constituent refrigerants [26-30]. Barbosa et al. [27] attempted to propose a non-equilibrium slug flow model to explain this behaviour found by Kandlbinder [26] in experiments with single-constituent refrigerants. Van den Bergh et al. [28] also tried to interpret the existence in their experiments with R245fa by using wetting of the top surface of the tube. Yet, the mechanism behind this peculiar behaviour found in flow boiling of zeotropic mixtures under the high pressure and high heat-flux experimental conditions in the present work needs further research.

Nucleate boiling suppression

In saturated boiling region, a temporary decline of heat-transfer coefficient at low quality has been noted. Greco [24,25] reported, in experiments with R407C and R410A, that high heat flux and high operating pressure affected the trend of heat-transfer coefficient and caused a local minimum occurring before intermediate quality, although absolute values of heat-transfer coefficient are lifted. Jung et al. [31] observed that the high heat-flux conditions could adversely lead to a temporary decrease of the heat-transfer coefficient of R22/R114 mixtures in the low-quality region.

A possible explanation for this result might be the suppression of nucleate boiling due to heat transfer resistance and mass transfer resistance. As flow boiling proceeds, the liquid phase gets enriched considerably in the less volatile components, as shown in Fig. 5 for R454B and Fig. 6 for R449A. A rise in amount of the less volatile components in liquid layer adjacent to the superheated wall surface would lift saturation temperature locally [18]. This inhibits temperature driving force from superheated surface to liquid and limits nucleate bubble growth on the surface in nucleate-dominated region. As shown in Fig.7, additional sensible heat is required to heat the remaining liquid

(rich in less volatile components) to a higher saturation temperature. Moreover, nucleate boiling is also suppressed by the mass transfer resistance. The more volatile components are preferentially evaporated at liquid/vapor interface while the less volatile components tend to remain in liquid side [31]. The increased concentration of less volatile components at liquid/vapor interface can result in a strong fraction gradient between liquid bulk and liquid/vapor interface. Consequently, a mass diffusion resistance owing to the fraction gradient would affect the evaporation rate adversely. In addition, flow boiling instability may also contribute to the temporary inhibition of heat transfer performance in the low-quality region.

Convective boiling

In moderate and high quality regions, it can be seen that the heat-transfer coefficient increases with vapor quality until the well-known partial dry-out occurs. Some studies [4, 24, 25, 32] suggested that, as vapor quality grows, the flow accelerates and hence the turbulence intensity is enhanced. It would lessen mass transfer resistance. Furthermore, as boiling proceeds, the liquid film becomes thinner and hence the thermal resistance is mitigated [24].

In addition, as vapor quality increases further, mixtures at moderate and high qualities would reflect more the liquid properties of the less volatile components as a consequence of composition shift illustrated in Fig.5 and Fig.6.

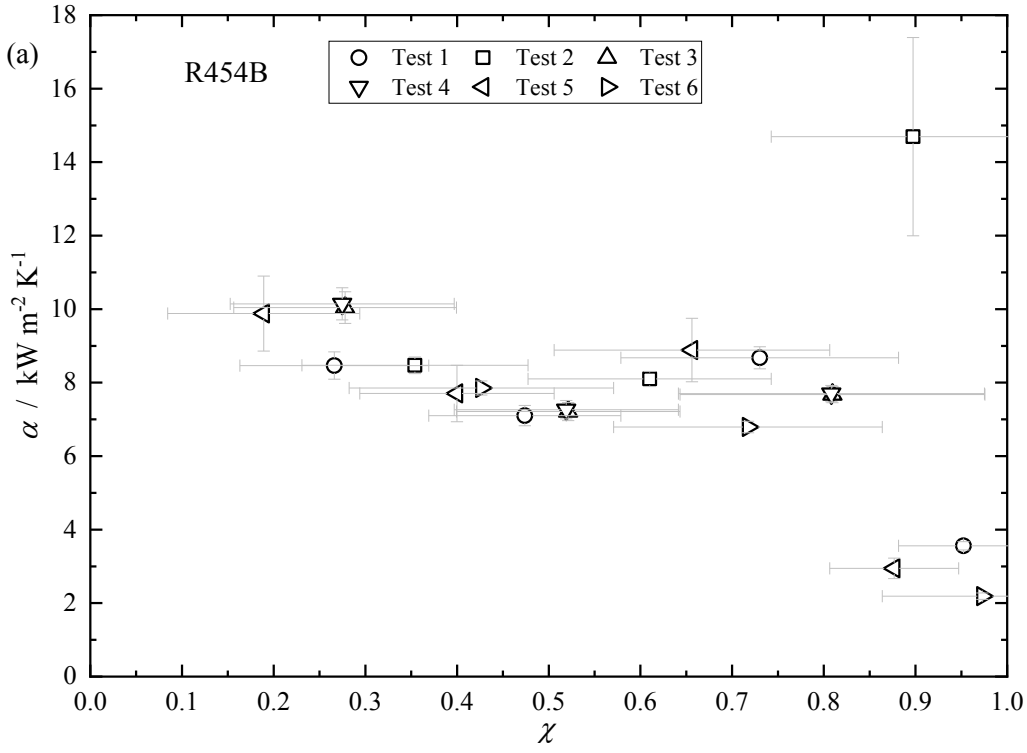

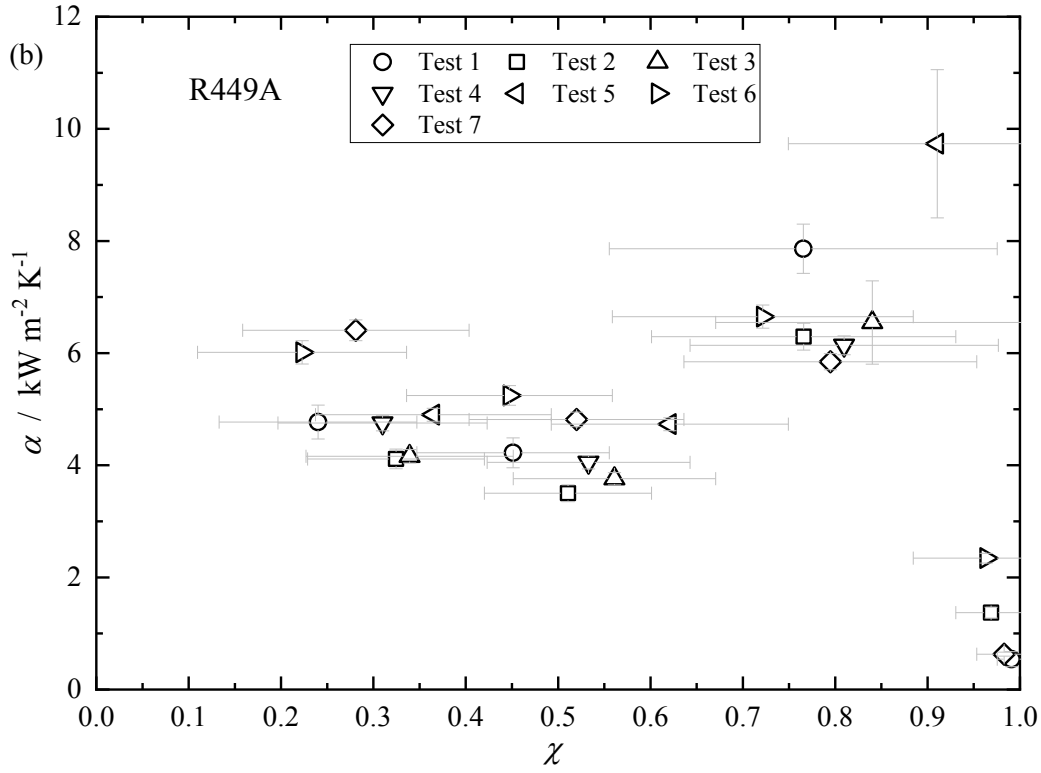

Fig.8 Measured flow boiling heat transfer coefficients of R454B and R449A against vapor quality in saturated boiling region. The horizontal bars indicate the vapor quality change in each subsection.

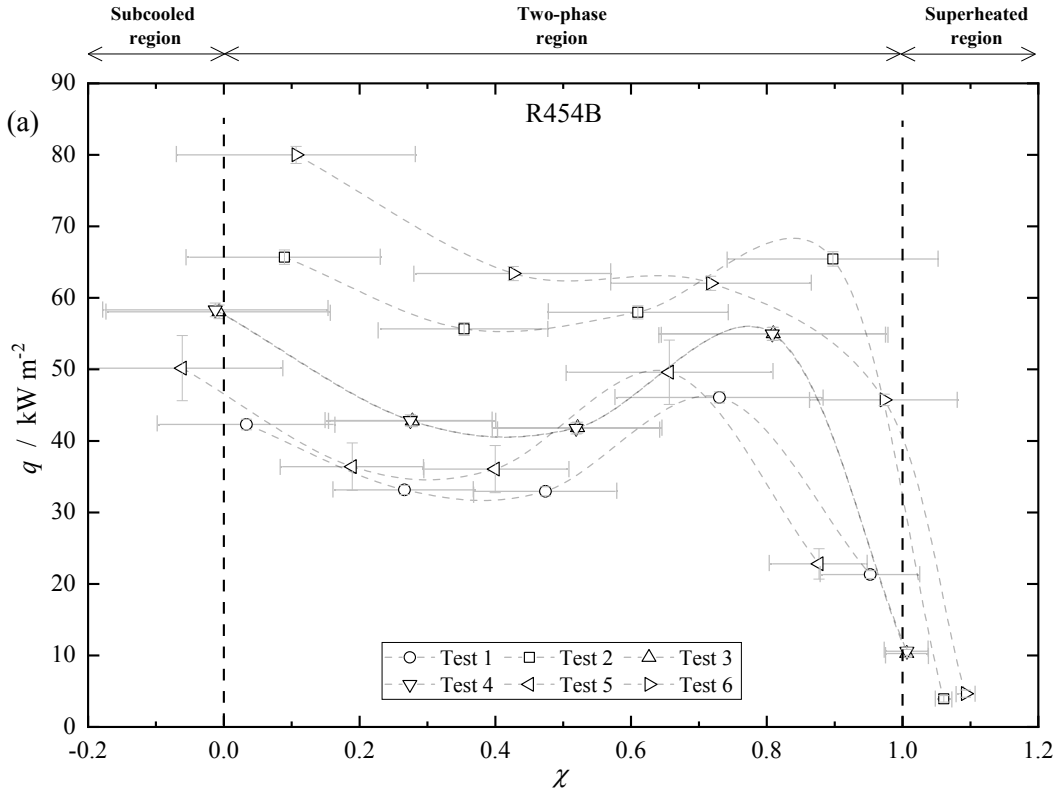

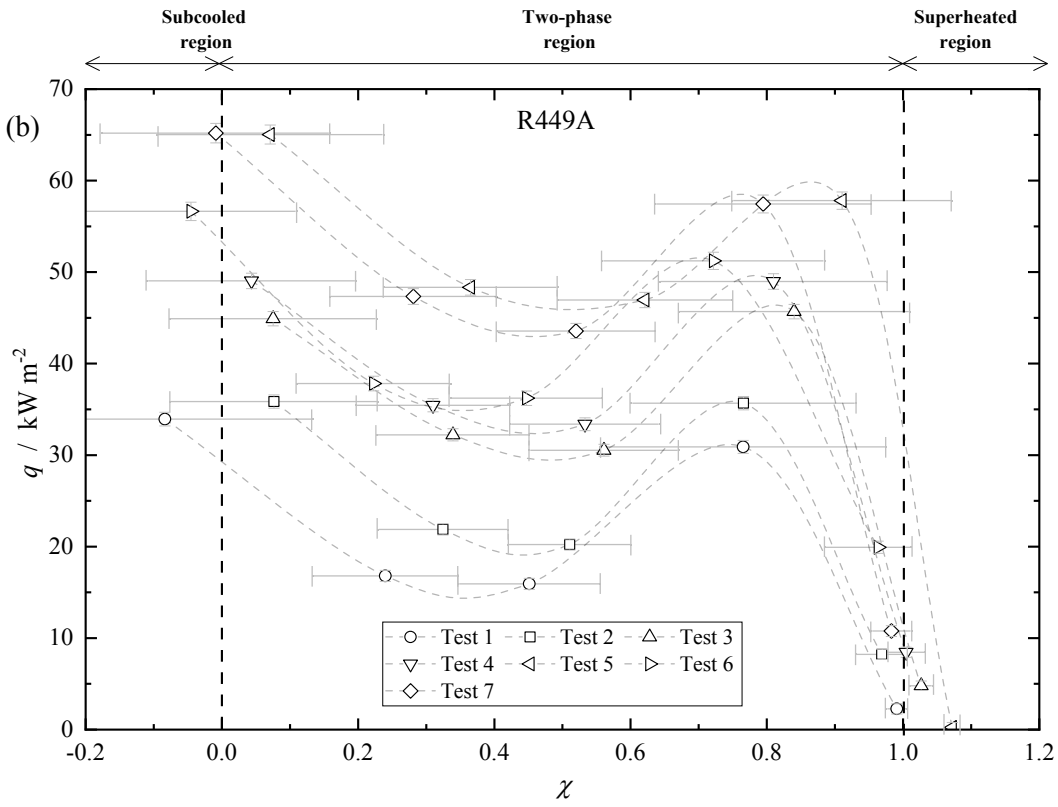

Fig.9 Measured flow boiling heat flux of R454B and R449A versus vapor quality. The horizontal bars indicate the vapor quality change in each subsection. The dashed line is a guide for eyes.

4. Conclusions

The local saturated flow boiling heat transfer of two refrigerant mixtures, R454B and R449A, inside a horizontal 8.7-mm ID smooth tube has been experimentally investigated. R454B is a binary mixture containing 68.9% of R32 and 31.1% of R1234yf by mass and R449A is a quaternary mixture including R32, R125, R1234yf and R134a (by mass 24.3%, 24.7%, 25.3% and 25.7%). Experiments have covered: mass flux from 201 kg m^{-2} s^{-1} to 269 kg m^{-2} s^{-1} and inlet pressure from 1.691 MPa to 3.282 MPa for R454B, mass flux ranging between 178 kg m^{-2} s^{-1} and 328.0 kg m^{-2} s^{-1} and inlet pressure ranging between 1.449 MPa and 3.244 MPa for R449A. The key findings of the present work are summarized below:

1. The variations of refrigerant temperature and local composition shift in vapor and liquid phases during flow boiling were studied. As the boiling process proceeds along the test tube, the refrigerant temperature increases with vapor quality. The more volatile constituents are richer in vapor than circulation composition of mixtures while less volatile constituents tend to remain in liquid phase. Thus, a fraction gradient and a temperature gradient may develop, which can create resistances to heat transfer.
2. R454B exhibited higher heat-transfer coefficient than R449A under similar experimental

conditions, which is presumably attributed to R454B's higher latent heat, higher liquid thermal conductivity, lower temperature glide and smaller molecular mass.

3. It was found that heat transfer peaks near zero vapor quality and decline gradually with increase of vapor quality in the nucleate boiling region. Then, after intermediate quality, heat-transfer coefficient tends to increase with vapor quality until the occurrence of partial dry-out. Possible explanations have been provided.

Acknowledgments

The authors would like to gratefully acknowledge the financial support from the Joint PhD Studentship of China Scholarship Council (CSC) and Queen Mary University of London, the supports of Super Radiator Coils Ltd., and Chemours for providing R454B refrigerant.

5. Appendix A

The uncertainty analysis in the present work was carried out referring to methodology presented in Kondou et al. [18].

A1. Uncertainty in pressure profiles

The uncertainties in pressure profiles are determined as the combination of local pressure and pressure drop, obtained by absolute pressure transducers and differential pressure transducers, respectively

$$\delta(P_{\mathrm{r,1in}}) = \delta(P_{\mathrm{r,1in}}) \text{ stemming from measurement}$$

$$\delta(P_{\mathrm{r,2in}}) = \delta(P_{\mathrm{r,1out}}) = \sqrt{\delta^2(P_{\mathrm{r,1in}}) + \delta^2(\Delta P_{\mathrm{r,1}})}$$

$$\vdots$$

$$\delta(P_{\mathrm{r,5out}}) = \sqrt{\delta^2(P_{\mathrm{r,5in}}) + \delta^2(\Delta P_{\mathrm{r,5}})} \tag{A.1}$$

A2. Uncertainties of $h_{r,1in}$

First, according to Kondou et al.[18], the uncertainty of specific enthalpy of refrigerant at the inlet of subsection 1, $h_{\mathrm{r,1in}}$, derived by measurements of pressure and temperature is determined as follows. The uncertainty of mixture composition is neglected.

$$\delta(h_{\mathrm{r,1in}}) \approx [\max(h_{\mathrm{r,1in}}) - \min(h_{\mathrm{r,1in}})]/2$$

$$\max(h_{\mathrm{r,1in}}) = \max\left[f\left(P_{\mathrm{r,1in}} \pm \delta(P_{\mathrm{r,1in}}), T_{\mathrm{r,1in}} \pm \delta(T_{\mathrm{r,1in}}), X_{\mathrm{c}}\right)\right]$$

$$\min(h_{\mathrm{r,1in}}) = \min\left[f\left(P_{\mathrm{r,1in}} \pm \delta(P_{\mathrm{r,1in}}), T_{\mathrm{r,1in}} \pm \delta(T_{\mathrm{r,1in}}), X_{\mathrm{c}}\right)\right] \tag{A.2}$$

A3. Uncertainty of the heat transfer rate to refrigerant for each subsection

$$\delta(Q_{r,1}) = \sqrt{[\delta(Q_{H_2O,1})]^2 + [\delta(Q_{loss,1})]^2}$$

$$\delta(Q_{H_2O,1}) = \sqrt{[(T_{H_2O,1in} - T_{H_2O,1out})\rho_{H_2O}c_{pH_2O}\delta(\dot{V}_{H_2O})]^2 + [\rho_{H_2O}\dot{V}_{H_2O}c_{pH_2O}\delta(T_{H_2O,1in})]^2 + [-\rho_{H_2O}\dot{V}_{H_2O}c_{pH_2O}\delta(T_{H_2O,1out})]^2}$$

⋮

$$\delta(Q_{r,5}) = \sqrt{[\delta(Q_{H_2O,5})]^2 + [\delta(Q_{loss,5})]^2}$$

$$\delta(Q_{H_2O,5}) = \sqrt{[(T_{H_2O,5in} - T_{H_2O,5out})\rho_{H_2O}c_{pH_2O}\delta(\dot{V}_{H_2O})]^2 + [\rho_{H_2O}\dot{V}_{H_2O}c_{pH_2O}\delta(T_{H_2O,5in})]^2 + [-\rho_{H_2O}\dot{V}_{H_2O}c_{pH_2O}\delta(T_{H_2O,5out})]^2}$$

(A.3)

A4. Uncertainty of refrigerant enthalpies along the test section (excluding $h_{r,1in}$)

$$\delta(h_{r,1out}) = \delta(h_{r,2in}) = \sqrt{[\delta(h_{r,1in})]^2 + [\frac{1}{\dot{m}_r} \times \delta(Q_{r,1})]^2 + [-Q_{r,1}\dot{m}_r{}^{-2}\delta(\dot{m}_r)]^2}$$

⋮

$$\delta(h_{r,4out}) = \delta(h_{r,5in}) = \sqrt{[\delta(h_{r,4in})]^2 + [\frac{1}{\dot{m}_r} \times \delta(Q_{r,4})]^2 + [-Q_{r,4}\dot{m}_r{}^{-2}\delta(\dot{m}_r)]^2}$$

$$\delta(h_{r,5out}) = \sqrt{[\delta(h_{r,5in})]^2 + [\frac{1}{\dot{m}_r} \times \delta(Q_{r,5})]^2 + [-Q_{r,5}\dot{m}_r{}^{-2}\delta(\dot{m}_r)]^2} \quad \text{(A.4)}$$

A5. Uncertainty related to representative refrigerant temperature for each subsection

$$\delta(T_{r,1}) = \sqrt{[\frac{1}{2}\delta(T_{r,1in})]^2 + [\frac{1}{2}\delta(T_{r,1out})]^2}$$

Where,

$\delta(T_{r,1in}) = \delta(T_{r,1in})$ caused by measurement

$\delta(T_{r,1out}) \approx [\max(T_{r,1out}) - \min(T_{r,1out})]/2$

$\max(T_{r,1out}) = \text{Max}\,[f(P_{r,1out} \pm \delta(P_{r,1out}), h_{r,1out} \pm \delta(h_{r,1out}), X_c)_{eqm}]$

$\min(T_{r,1out}) = \text{Min}\,[f(P_{r,1out} \pm \delta(P_{r,1out}), h_{r,1out} \pm \delta(h_{r,1out}), X_c)_{eqm}]$

⋮

$$\delta(T_{r,5}) = \sqrt{[\frac{1}{2}\delta(T_{r,5in})]^2 + [\frac{1}{2}\delta(T_{r,5out})]^2}$$

where,

$\delta(T_{r,5in}) \approx [\max(T_{r,5in}) - \min(T_{r,5in})]/2$

$\max(T_{r,5in}) = \text{Max}\,[f(P_{r,5in} \pm \delta(P_{r,5in}), h_{r,5in} \pm \delta(h_{r,5in}), X_c)_{eqm}$

$$\min(T_{\mathrm{r,5in}}) = \mathrm{Min}\,[f(P_{\mathrm{r,5in}} \pm \delta(P_{\mathrm{r,5in}}), h_{\mathrm{r,5in}} \pm \delta(h_{\mathrm{r,5in}}), X_{\mathrm{c}})_{\mathrm{eqm}}$$

$$\delta(T_{\mathrm{r,5out}}) \approx [\max(T_{\mathrm{r,5out}}) - \min(T_{\mathrm{r,5out}})]/2$$

$$\max(T_{\mathrm{r,5out}}) = \mathrm{Max}\,[f(P_{\mathrm{r,5out}} \pm \delta(P_{\mathrm{r,5out}}), h_{\mathrm{r,5out}} \pm \delta(h_{\mathrm{r,5out}}), X_{\mathrm{c}})_{\mathrm{eqm}}$$

$$\min(T_{\mathrm{r,5out}}) = \mathrm{Min}\,[f(P_{\mathrm{r,5out}} \pm \delta(P_{\mathrm{r,5out}}), h_{\mathrm{r,5out}} \pm \delta(h_{\mathrm{r,5out}}), X_{\mathrm{c}})_{\mathrm{eqm}} \quad \text{(A.5)}$$

The uncertainty related to vapor quality and local compositions of mixtures in liquid phase and vapor phase are all estimated in a similar way to the representative refrigerant temperature.

A6. Uncertainty of outer and inner wall temperatures

$$\delta(T_{\mathrm{wo}})^2 = [\frac{1}{8}\delta(T_{\mathrm{wo,top1}})]^2 + [\frac{1}{8}\delta(T_{\mathrm{wo,top2}})]^2 + [\frac{1}{8}\delta(T_{\mathrm{wo,bot1}})]^2 + [\frac{1}{8}\delta(T_{\mathrm{wo,bot2}})]^2 + [\frac{1}{8}\delta(T_{\mathrm{wo,right1}})]^2 + [\frac{1}{8}\delta(T_{\mathrm{wo,right2}})]^2 + [\frac{1}{8}\delta(T_{\mathrm{wo,left1}})]^2 + [\frac{1}{8}\delta(T_{\mathrm{wo,left2}})]^2$$

$$\delta(T_{\mathrm{wi}}) = \sqrt{[\delta(T_{\mathrm{wo}})]^2 + [-\frac{1}{2\pi\lambda_{\mathrm{w}}\Delta z} ln\frac{d_{\mathrm{o}}}{d_{\mathrm{i}}} \times \delta(Q_{\mathrm{r}})]^2} \quad \text{(A.6)}$$

The uncertainties in tube diameter, length of subsections, and thermal conductivity of tube are neglected in this case.

A7. Uncertainty in heat fluxes and heat transfer coefficient

$$\delta(q) = \frac{1}{A}\delta(Q_{\mathrm{r}})$$

$$\delta(\alpha) = \sqrt{[\frac{1}{T_{\mathrm{wi}} - T_{\mathrm{r}}} \times \delta(q)]^2 + [-q(T_{\mathrm{wi}} - T_{\mathrm{r}})^{-2} \times \delta(T_{\mathrm{wi}})]^2 + [q(T_{\mathrm{wi}} - T_{\mathrm{r}})^{-2} \times \delta(T_{\mathrm{r}})]^2} \quad \text{(A.7)}$$

A8. Expanded uncertainty

The expanded uncertainty that assures a 95% confidence level is obtained by multiplying the uncertainties above by a coverage factor CF=2. The expanded uncertainty of heat transfer coefficient is shown below as instance:

$$\delta(\alpha)_{\mathrm{expanded}} = 2 \times \delta(\alpha) \quad \text{(A.8)}$$

6. References

1. Calm, J. M. 2008. The next generation of refrigerants – Historical review, considerations, and outlook. International Journal of Refrigeration, 31, 1123-1133.
2. McLinden, M. O., Kazakov, A. F., Brown, J. S., and Domanski, P. A. 2014. A thermodynamic analysis of refrigerants: Possibilities and tradeoffs for Low-GWP refrigerants. International Journal of Refrigeration, 38, 80-92.
3. Azzolin, M., Bortolin, S., and Del Col, D. 2016. Predicting methods for flow boiling heat transfer of a non-azeotropic mixture inside a single microchannel. Heat Transfer Engineering,

37(13-14), 1136-1147.

4. Jige, D., Kikuchi, S., Mikajiri, N. and Inoue, N. 2020. Flow boiling heat transfer of zeotropic mixture R1234yf/R32 inside a horizontal multiport tube. International Journal of Refrigeration, 119, 390-400.
5. 2018 United Nations Environment Programme. Refrigeration, Air Conditioning, & Heat Pumps Technical Options Committee. 2018 Report of the Refrigeration, Air Conditioning, and Heat Pumps Technical Options Committee: 2018 Assessment.
6. Rajapaksha, L. 2007. Influence of special attributes of zeotropic refrigerant mixtures on design and operation of vapour compression refrigeration and heat pump systems. Energy conversion and Management, 48(2), 539-545
7. Azzolin, M., Bortolin, S., and Del Col, D. 2016. Flow boiling heat transfer of a zeotropic binary mixture of new refrigerants inside a single microchannel. International Journal of Thermal Sciences, 110, 83-95.
8. Didion, D. A., and Bivens, D. B. 1990. Role of refrigerant mixtures as alternatives to CFCs. International Journal of Refrigeration, 13(3), 163-175.
9. Mastrullo, R., Mauro, A. W. and Viscito, L. 2019. Flow boiling of R452A: Heat transfer data, dry-out characteristics and a correlation. Experimental Thermal and Fluid Science, 105, 247-260.
10. Wantha, C. 2019. Analysis of heat transfer characteristics of tube-in-tube internal heat exchangers for HFO-1234yf and HFC-134a refrigeration systems. Applied Thermal Engineering, 157, 113747.
11. Navarro-Esbrí, J., Mendoza-Miranda, J. M., Mota-Babiloni, A., Barragán-Cervera, A., and Belman-Flores, J. M. 2013. Experimental analysis of R1234yf as a drop-in replacement for R134a in a vapor compression system. International Journal of Refrigeration, 36(3), 870-880.
12. Cho, H., Lee, H. and Park, C. 2013. Performance characteristics of an automobile air conditioning system with internal heat exchanger using refrigerant R1234yf. Applied Thermal Engineering, 61, 563-569.
13. Li, M., Dang, C. and Hihara, E. 2012. Flow boiling heat transfer of HFO1234yf and R32 refrigerant mixtures in a smooth horizontal tube: Part I. Experimental investigation. International Journal of Heat and Mass Transfer, 55, 3437-3446.
14. Lillo, G., Mastrullo, R., Mauro, A. W., Pelella, F. and Viscito, L. 2019. Experimental thermal and hydraulic characterization of R448A and comparison with R404A during flow boiling. Applied Thermal Engineering, 161,114146.
15. Berto, A., Azzolin, M., Bortolin, S., Guzzardi, C. & Del Col, D. 2020. Measurements and

modelling of R455A and R452B flow boiling heat transfer inside channels. International Journal of Refrigeration, 120, 271-284.

16. Lemmon, E.W., Bell, I.H., Huber, M.L., McLinden, M.O. NIST Standard Reference Database 23: Reference Fluid Thermodynamic and Transport Properties-REFPROP, Version 10.0, National Institute of Standards and Technology, Standard Reference Data Program, Gaithersburg, 2018.
17. Shao, D. W., and Granryd, E. 1998. Experimental and theoretical study on flow condensation with non-azeotropic refrigerant mixtures of R32/R134a. International journal of refrigeration, 21(3), 230-246.
18. Kondou, C., BaBa, D., Mishima, F., and Koyama, S. 2013. Flow boiling of non-azeotropic mixture R32/R1234ze (E) in horizontal microfin tubes. International Journal of Refrigeration, 36(8), 2366-2378.
19. Taylor, J. 1997. Introduction to error analysis, the study of uncertainties in physical measurements.
20. Moffat, R. J. 1988. Describing the uncertainties in experimental results. Experimental thermal and fluid science, 1(1), 3-17.
21. ASME, 2005, Test Uncertainty, ASME PTC 19.1-2005.
22. Azzolin, M., Berto, A., Bortolin, S., Moro, L., and Del Col, D. 2019. Condensation of ternary low GWP zeotropic mixtures inside channels. International Journal of Refrigeration, 103, 77-90.
23. Kim, S. M., and Mudawar, I. 2013. Universal approach to predicting saturated flow boiling heat transfer in mini/micro-channels–Part I. Dryout incipience quality. International Journal of Heat and Mass Transfer, 64, 1226-1238.
24. Greco, A. 2008. Convective boiling of pure and mixed refrigerants: an experimental study of the major parameters affecting heat transfer. International Journal of Heat and Mass Transfer, 51(3-4), 896-909.
25. Greco, A. 2010. Convective Boiling Heat Transfer of Pure and Mixed Refrigerants within Plain Horizontal Tubes: An Experimental Study. Advances in Multiphase Flow and Heat Transfer, 2, 216.
26. Kandlbinder, T. 1997. Experimental investigation of forced convective boiling of hydrocarbon and hydrocarbon mixtures. Ph. D. Thesis, University of London (Imperial College).
27. Barbosa Jr, J. R., and Hewitt, G. F. 2005. A thermodynamic nonequilibrium slug flow model. J. Heat Transfer, 127(3), 323-331.

28. Van den Bergh, W. J., Moran, H. R., Dirker, J., Markides, C. N., and Meyer, J. P. 2021. Effect of low heat and mass fluxes on the boiling heat transfer coefficient of R-245fa. International Journal of Heat and Mass Transfer, 180, 121743.
29. Vakili-Farahani, F., Agostini, B., and Thome, J. R. 2013. Experimental study on flow boiling heat transfer of multiport tubes with R245fa and R1234ze (E). International journal of refrigeration, 36(2), 335-352.
30. You, X. Y., Liu, J. H., Hua, N., Wang, J., Xu, R. J., Yu, G. X., and Wang, H. S. 2021. Experimental study on flow boiling of refrigerant R1233zd (E) in microchannels: Heat transfer. Applied Thermal Engineering, 182, 116083.
31. Jung, D. S., McLinden, M., Radermacher, R., and Didion, D. 1989. Horizontal flow boiling heat transfer experiments with a mixture of R22/R114. International journal of heat and mass transfer, 32(1), 131-145.
32. Azzolin, M., and Bortolin, S. 2021. Condensation and flow boiling heat transfer of a HFO/HFC binary mixture inside a minichannel. International Journal of Thermal Sciences, 159, 106638.